

# Battery Energy Storage System Models for Microgrid Stability Analysis and Dynamic Simulation

Mostafa Farrokhabadi, *Student Member, IEEE*, Sebastian König, Claudio Cañizares, *Fellow, IEEE*,  
Kankar Bhattacharya, *Fellow, IEEE*, and Thomas Leibfried, *Member, IEEE*

**Abstract**—With the increasing importance of battery energy storage systems (BESS) in microgrids, accurate modeling plays a key role in understanding their behaviour. This paper investigates and compares the performance of BESS models with different depths of detail. Specifically, several models are examined: an average model represented by voltage sources; an ideal dc source behind a voltage source converter; a back-to-back buck/boost and bi-directional three phase converter, with all models sharing the same control system and parameters; and two additional proposed models where the switches are replaced by dependent sources to help analyze the differences observed in the performance of the models. All these models are developed in PSCAD and their performances are simulated and compared considering various issues such as voltage and frequency stability and total harmonic distortion, in a benchmark test microgrid. It is shown through simulation results and eigenvalue studies that the proposed models can exhibit different performance, especially when the system is heavily loaded, highlighting the need for more accurate modeling under certain microgrid conditions.

**Index Terms**—Energy storage systems, dynamic simulation, microgrids, modeling, stability.

## I. INTRODUCTION

MICROGRIDS are defined as a cluster of interconnected distributed energy resources (DERs), energy storage systems (ESS), and loads which can operate in parallel with the grid or in an islanded mode [1]. Under the smart grid paradigm, microgrids are considered a critical link in the evolution from vertically integrated bulk power systems to smart decentralized distribution networks [2], with high penetration of renewables, easily scalable structures, and increased reliability levels [3]. However, such active distribution networks present various challenges, such as the integration of plug-in electric vehicles and the proliferation of renewable energy sources (RES), which have to be addressed when significant penetration levels are reached [4]. In this context, BESS can be practically helpful to deal with such challenges, as explained next.

This work has been partially supported by NSERC-Canada through Discovery Grants.

M. Farrokhabadi, C. A. Cañizares, and K. Bhattacharya are with the Department of Electrical and Computer Engineering, University of Waterloo, Waterloo, ON N2L 3G1, Canada (e-mail: m5farrok@uwaterloo.ca; ccanizares@uwaterloo.ca; kankar@ece.uwaterloo.ca).

S. Koenig and T. Leibfried are with Institute of Electric Energy Systems and High-Voltage Technology (IEH), Karlsruhe Institute of Technology, Karlsruhe, Germany (e-mail: sebastian.koenig@kit.edu; thomas.leibfried@kit.edu).

For several interesting technical features, BESS have received considerable attention recently, particularly as a solution to the challenges facing modern active distribution networks and microgrids. BESS can provide several key ancillary services, such as load shifting, dynamic local voltage support, short-term frequency smoothing, grid contingency support, and reduce the need for fossil-fuel-based generation [4], [5]. Therefore, BESS are considered a key enabling element of modern smart grids and microgrids.

Since many utilities and researchers use simulation software packages to model and investigate various issues in microgrids, grid components need to be adequately modeled to properly reflect the behaviour and performance of the system. Several components of microgrids have been extensively studied, and a variety of models have been developed and reported in the literature. However, since inverter-based BESS are relatively new elements of microgrids, fewer studies have been conducted on their modeling and control. In [6], a generalized mathematical model of ESS is presented for voltage and angle stability analysis based on the balanced fundamental-frequency model of the Voltage Source Converter (VSC) and the dynamics of the dc link, based on a set of linear differential algebraic equations. However, the impact of inverter switching on the system performance is not modeled, and the performance of the proposed model under different microgrid conditions such as heavy and/or unbalanced loading are not studied. Detailed ESS models for transient analysis in microgrids are presented in [5] and [7]. However, the focus of these papers is on ESS applications in microgrids, without considering the impact of ESS modeling on the system dynamic performance. Simplified models of ESS are presented in [8] and [9], but similar to the aforementioned papers, they dwell on applications of ESS in power systems rather than the modeling of ESS; the ESS models consist of only active and reactive power loops, neglecting VSC and dc link circuits, and the ESS dynamic performance.

Considering the variety of BESS components, such as dc-dc and dc-ac converters, studies on the impact of level of detail in BESS modeling on the stability and dynamic performance of microgrids have not yet been reported in the literature. Hence, considering the importance of BESS in active distribution networks and microgrids, this paper investigates and compares microgrid dynamic performance using BESS models with different depth of detail. Specifically, several models are studied: an average model represented by voltage sources [10]; an ideal

dc source behind a voltage source converter [11]; and a back-to-back buck/boost and bi-directional three phase converter [12], with all models sharing the same control systems and parameters; and two additional proposed models where the switches are replaced by dependent sources to help analyzing the differences observed in the performance of the models. The models are developed in PSCAD and their performance is compared considering various variables such as voltages and currents at the point-of-common-coupling, active and reactive power injection, and total harmonic distortion, in the context of the impact on the the stability of the system. Thus, the main objectives and contributions of the paper are the following:

- Develop and study various BESS models for microgrid simulation and analysis, including a new and efficient model where the switches are replaced by dependent sources, identifying the conditions in which each model can be used. A systematic mechanism is applied to isolate and evaluate the impact of various parameters.
- For the first time, study the impact of BESS converter switching on microgrid stability, including high-frequency signals and internal resistances of switches.
- Study the impact of BESS dc link voltage dynamics on microgrid stability, through eigenvalue studies and dynamic simulations.
- Study and demonstrate the impact of unbalanced loading on microgrids stability.
- Compare the performance of the proposed models in a realistic test microgrid, determining their advantages and limitations, and their computational efficiency.

The rest of this paper is organized as follows: Section II describes the various components and parameters used to model BESS in detail, and Section III presents three approximated models to approximately represent BESS in dynamic system studies. Case studies and simulation results are presented in Section IV, comparing the performance of BESS models with different depth of detail. Section V analyzes in detail the reasons for the differences observed in the performance of the various models presented. Finally, the main findings and conclusions of the studies presented in the paper are provided in Section VI.

## II. BESS DETAILED MODEL

The BESS models used in this paper mainly include a buck/boost converter, a dc link capacitor, a three-phase bi-directional dc-ac converter, an ac filter, and a transformer connecting the system to the microgrid. In this section, these models and the corresponding parameters are discussed, and the control techniques used for each BESS converter are also described. Figure 8 depicts in detail the BESS components [5].

### A. Battery

The battery model described here is based on the generic model proposed in [13], and is modeled as a controllable ideal dc source in series with an internal resistance  $R_B$ . The no-load voltage of the battery  $E_B$  is calculated based on the state-of-charge (SOC) of the battery using a nonlinear equation, as follows:

$$E_B = E_0 - K \frac{1}{SOC} + A^{-BQ(1-SOC)} \quad (1)$$

where  $E_0$  is the battery constant voltage in V,  $K$  is the polarization voltage in V,  $Q$  is the battery capacity in Ah, and  $A$  and  $B$  are parameters determining the charge and discharge characteristics of the battery. The parameters  $A$ ,  $B$ , and  $K$  can be tuned to mimic a specific battery type discharge characteristic.

Note that the time frame of the test scenarios discussed in this paper is in the order of a few seconds; hence, since the BESS designed and simulated in this paper has a rated power of 1 MW and a rated capacity of 1 MWh, which is a typical power to capacity ratio for BESS in microgrids, the battery voltage and SOC relation cannot be observed in the presented simulation results.

### B. Buck/Boost Converter

The buck/boost converter is in charge of controlling the dc link capacitor voltage by properly charging and discharging the battery. A cascaded PI controller is used here to generate the duty cycle for the switches based on the difference of the dc link voltage and its set-point, as shown in Fig. 2. Note that the second PI controller reacts to changes in the active power of the system first, thus improving the ability of the buck/boost controller to maintain the dc link voltage.

When the dc link voltage is lower than the pre-defined set-point, the converter works in the boost mode, discharging the battery. When the dc link voltage is higher than the set-point, the converter operates in the buck mode, charging the battery. The current ripple is bounded by a proper choice of the inductor  $L_{chopf}$ , as follows [14]:

$$\Delta I = \frac{E_B}{L_{chopf}} \Delta t = \frac{E_B}{L_{chopf}} \frac{1}{2f_s} \quad (2)$$

where  $f_s$  is the switching frequency.

### C. DC-AC Converter

Figure 8 illustrates how the dc-ac converter connects the battery and buck/boost converter to the grid through the ac filter. The converter control system provides the voltage magnitude and phase set-points to create sinusoidal reference signals for the Pulse Width Modulation (PWM) scheme of the converter.

As shown in Fig. 8, when the switches are in State 1, the voltage magnitude and phase set-points are obtained based on the reference voltage and frequency; thus, the BESS in this case is the master voltage and frequency controller of the system, which is referred to as a grid-forming control technique. If the switches are in State 2, the voltage magnitude and phase set-points are obtained based on the reference active and reactive powers; hence, the battery is operated in constant  $PQ$  mode, injecting/absorbing constant active and reactive power, which is referred to as grid-feeding mode. Grid-supporting and grid-following control modes are based on these two fundamental control strategies, and are accomplished by changing the reference voltage, frequency, active power,

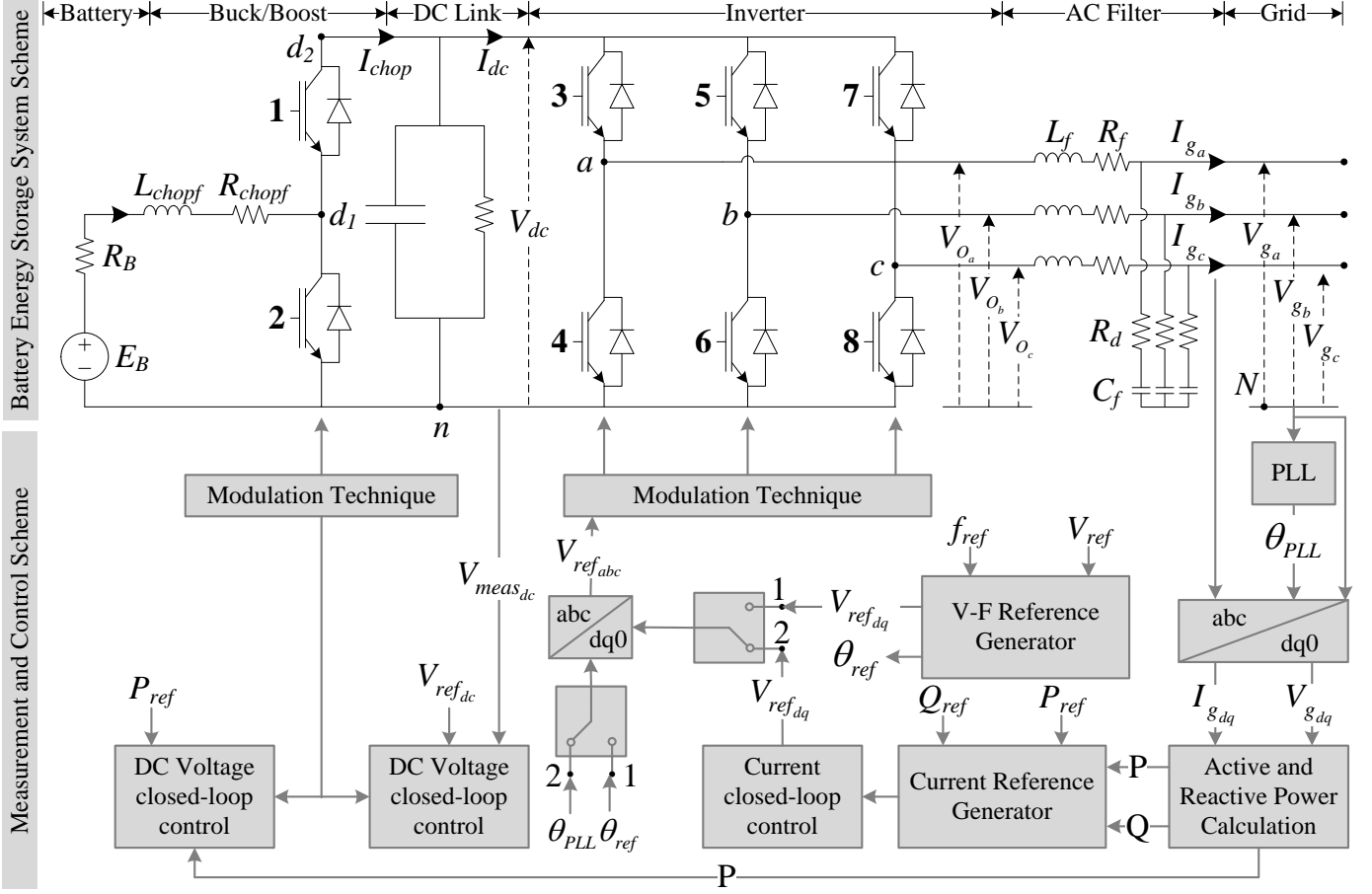


Fig. 1. Schematic of a battery energy storage system components and its controls [5].

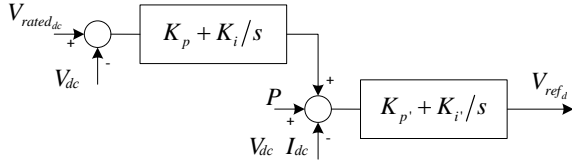


Fig. 2. Buck/boost dc link voltage controller.

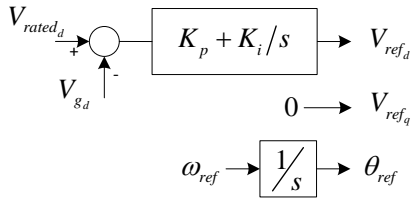


Fig. 3. Grid-forming voltage and phase reference generator.

and/or reactive power [15]. Observe that these controls are based on Park's dq-axes transformations.

In the grid-forming mode, the voltage dq-axes reference set-points would be directly used to create the abc-reference signals, as shown in Fig. 3. The reference angle is obtained by integrating the reference angular frequency. Observe that a PI controller is used to maintain the point of common coupling (PCC) voltage at its rated value.

In grid-feeding control mode, the injected active and reactive power are calculated first, as follows:

$$p = \frac{3}{2} (V_{gd} I_{gd} - V_{gq} I_{gq}) \quad (3)$$

$$q = \frac{3}{2} (V_{gd} I_{gq} - V_{gq} I_{gd}) \quad (4)$$

To obtain the corresponding fundamental  $P$  and  $Q$  components, the instantaneous active  $p$  and reactive  $q$  powers are passed through low-pass filters. The fundamental active and reactive powers are then passed through the current reference generator block to obtain the current dq-axes reference set-points, as follows:

$$I_{ref_d} = \frac{2}{3} \frac{P_{ref} V_{gd} + Q_{ref} V_{gq}}{V_{gd}^2 + V_{gq}^2} \quad (5)$$

$$I_{ref_q} = \frac{2}{3} \frac{P_{ref} V_{gq} - Q_{ref} V_{gd}}{V_{gd}^2 + V_{gq}^2} \quad (6)$$

These current references are then passed through the current closed-loop control to obtain the final voltage dq-axes references; feed-forward terms should be used to decouple the two axes, and should be considered for the difference between the voltages after and before the ac filter. Neglecting  $R_d$ , a single line diagram can be used to derive such a relation, as shown in Fig. 4, resulting in the following equations:

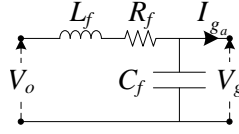


Fig. 4. Single line diagram of ac filter.

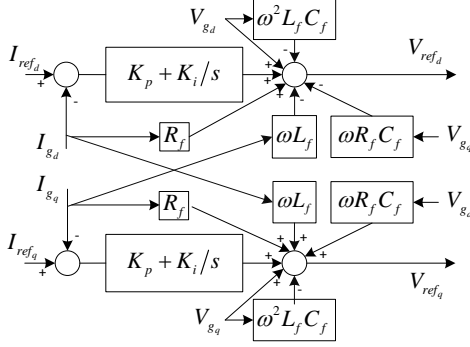


Fig. 5. Current closed-loop control.

$$V_{od} = V_{gd}(1 - \omega^2 L_f C_f) + I_{gd} R_f - I_{gq} \omega L_f - V_{gq} \omega R_f C_f \quad (7)$$

$$V_{oq} = V_{gq}(1 - \omega^2 L_f C_f) + I_{gd} R_f + I_{gd} \omega L_f + V_{gd} \omega R_f C_f \quad (8)$$

The final current closed-loop control block shown in Fig. 5 can be obtained from these equations.

The output of the current controller are the voltage references  $V_{ref_d}$  and  $V_{ref_q}$ , which are transformed back to the abc-reference frame to obtain the sinusoidal control signals for PWM scheme of the converter. More information on alternative converter controls such as grid-supporting and grid-following can be found in [15].

#### D. AC Filter

The ac filter should be designed properly to limit output current ripple and achieve an acceptable damping rate. The ac filter inductor  $L_f$  in a dc-ac converter can be determined based on the maximum acceptable current ripple, the dc link voltage, and the switching frequency as follows [16]:

$$\Delta I_{max} = \frac{V_{dc}/3}{L_f 4f_s} \quad (9)$$

The ac filter capacitor  $C_f$  reactive power injection has to be less than 5% of the converter rated power [16]. A series damping resistance is considered to prevent harmonic oscillations, and is assumed to consume 0.2% of the rated power as per:

$$R_d = \frac{V_I^2}{0.002 P_I} - \sqrt{\left( \frac{V_I^2}{0.002 P_I} \right)^2 - \frac{1}{(\omega C_f)^2}} \quad (10)$$

Also, a resistance  $R_f$  is added in series with the filter inductance to represent its parasitic resistance losses.

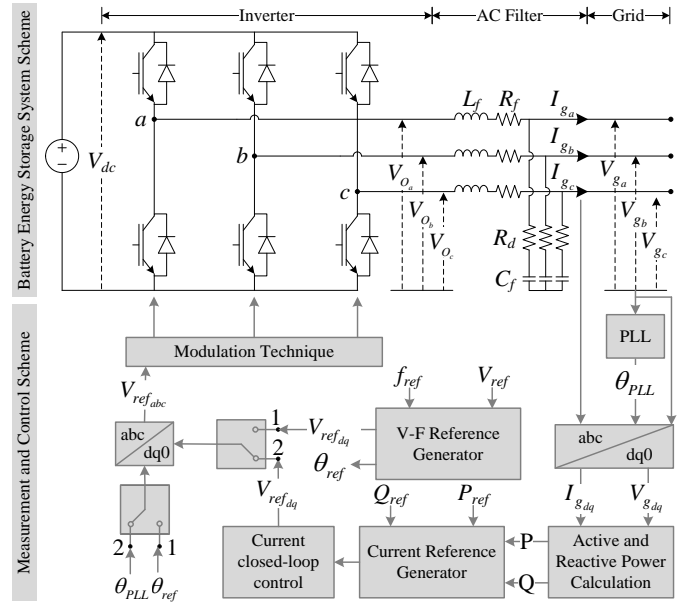


Fig. 6. Ideal dc link model of the BESS.

### III. ESS APPROXIMATE MODELS

In the previous section, the different BESS components and their corresponding controls are discussed in detail. Models have been proposed in the literature, in which some components of the detailed BESS model are eliminated to achieve faster simulation speed and/or reduce control complexity, as explained next.

#### A. Ideal DC Link Model

The schematic of this model is shown in Fig. 6, where the battery model along with the buck-boost converter is replaced by an ideal dc source, thus fixing the dc link voltage. Hence, the controls related to the dc link are eliminated. The rest of the system remains the same, i.e. the inverter and the ac filter and the corresponding control are the same as explained in Section II.

#### B. Average Model

The schematic of this model is shown Fig. 7, where the entire switching system is replaced by ideal voltage sources, i.e. the battery, buck-boost converter, and dc-ac inverter are eliminated; this increases the simulation speed significantly. The control system for the battery remains the same as in Section II; the only change is that abc-reference signals are directly fed to the ideal voltage sources, and the PWM scheme controls are eliminated.

#### C. Dependent Source Model (DSM)

To identify and isolate the impact of switches on the performance of the system, a model is proposed here in which the switches are replaced by dependent voltage and current sources, as shown in Fig. 8. The control system remains the same as in Fig. 1. Two models are developed based on the value of the dependent voltage and current sources, as explained next.

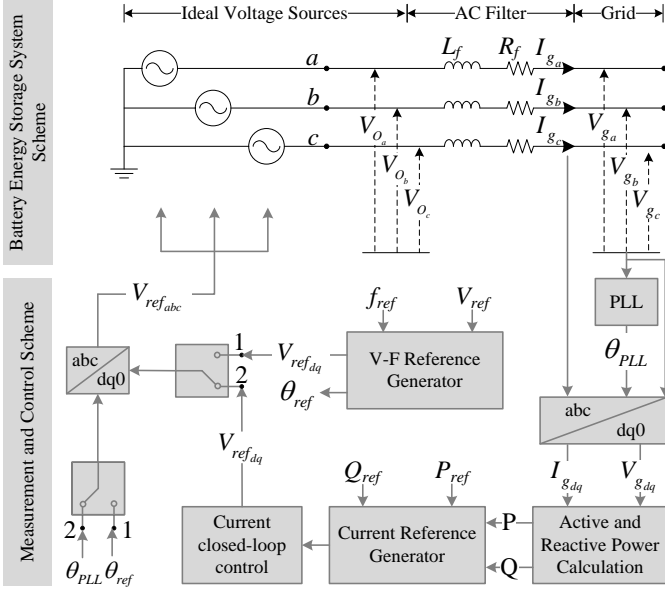


Fig. 7. Average model of the BESS.

1) *Switching DSM*: To emulate the performance of the model with switches, the currents through and voltages across the switches are analyzed in each switching state. For the buck/boost converter, when Switch 1 is on and Switch 2 is off in Fig. 1,  $V_{d1n} = V_{dc}$ , and the current through Switch 1 is  $I_{chop}$ . Hence,  $V_B$  and  $I_B$  in Fig. 8, can be defined as follows:

$$V_{d1n} = V_B = D_{S1} V_{dc} \quad (11)$$

$$I_B = D_{S1} I_{chop} \quad (12)$$

where  $D_{S1}$  is the duty cycle of Switch 1.

For the dc-ac inverter, when Switch 3 is on and Switch 4 is off,  $V_{an} = V_{dc}$ , and the current through Switch 3 is  $I_{ga}$ . Thus,  $V_a$  and  $I_a$  in Fig. 8 can be defined as follows:

$$V_{an} = D_{S3} V_{dc} \quad (13)$$

$$I_a = D_{S3} I_{ga} \quad (14)$$

where  $D_{S3}$  is the duty cycle of Switch 3. Similarly for the other two legs of the inverter. Note that the internal resistances of switches are modelled by  $R_{in}$ .

2) *Average DSM*: To eliminate the impact of high-frequency switching, an averaging technique based on the fundamental frequency component is used here. Thus, by assuming that no current goes through  $C_f$  in Fig. 1 and using KVL, the following equations can be derived:

$$\begin{aligned} V_{an} &= R_f I_{ga} + L_f \frac{dI_{ga}}{dt} + V_{ga} + V_{nN} \\ V_{bn} &= R_f I_{gb} + L_f \frac{dI_{gb}}{dt} + V_{gb} + V_{nN} \\ V_{cn} &= R_f I_{gc} + L_f \frac{dI_{gc}}{dt} + V_{gc} + V_{nN} \end{aligned} \quad (15)$$

A  $\Delta$ -Y transformer usually connects the the inverter to the rest of the grid, thus:

$$\begin{aligned} V_{ga} + V_{gb} + V_{gc} &= 0 \\ I_{ga} + I_{gb} + I_{gc} &= 0 \end{aligned} \quad (16)$$

Based on (15) and (16) the following equation can be obtained:

$$V_{aN} = V_{an} + V_{nN} = V_{an} - \frac{V_{an} + V_{bn} + V_{cn}}{3} \quad (17)$$

Similarly for the voltage on the other phases. In addition,  $D_{S3}$  in (13) and (14) can be replaced by its low-frequency contents, i.e., its local average, as follows [17]:

$$D_{S3_{avg}} = \frac{1}{2} + \frac{1}{2} m_a \quad (18)$$

where  $m_a$  is the modulating signal used to control  $D_{S3}$ , normalized to the peak value of the carrier signal. Thus, from (17) and (18), the dependent source in phase  $a$  can be defined as follows:

$$\begin{aligned} V_{aN_{avg}} &= \left( \frac{1}{2} + \frac{1}{2} m_a \right) V_{dc} - \\ &\frac{\frac{3}{2} + \frac{1}{2}(m_a + m_b + m_c)}{3} V_{dc} = \frac{1}{2} m_a V_{dc} \end{aligned} \quad (19)$$

And similarly for the dependent voltage sources in the other phases.

Finally, using KCL, the following equation can be obtained:

$$I_{dc} = I_a + I_b + I_c \quad (20)$$

Thus, based on (20), (18), and (16), the dependent current source in phase  $a$  can be defined as follows:

$$I_{a_{avg}} = \frac{1}{2} m_a I_{ga} \quad (21)$$

And similarly for the current source in the other phases.

#### IV. RESULTS

To effectively compare the performance of the three different modeling approaches, a test system based on the CIGRE benchmark for medium voltage distribution network introduced in [18] is implemented in PSCAD/EMTDC, as shown in Fig. 9. The test system has a 1.3 MVA diesel-based synchronous machine, a 1 MW BESS, and a 1 MW wind turbine, with the latter being modeled using an average model similar to Fig. 7, and operated as a constant power source for the short duration of time it is connected to the grid, since the disconnection of the wind turbine is used here as a disturbance. The diesel-based synchronous machine and its exciter and governor are tuned and validated according the actual measurements from a commercial grade synchronous machine in [19]. The BESS design parameters are shown in Table I. The loads are modeled using a voltage-sensitive exponential model with a 1.5 exponent, which is a reasonable value for typical isolated microgrids [20]. The load demand and unbalance levels are different for each test scenario discussed next.

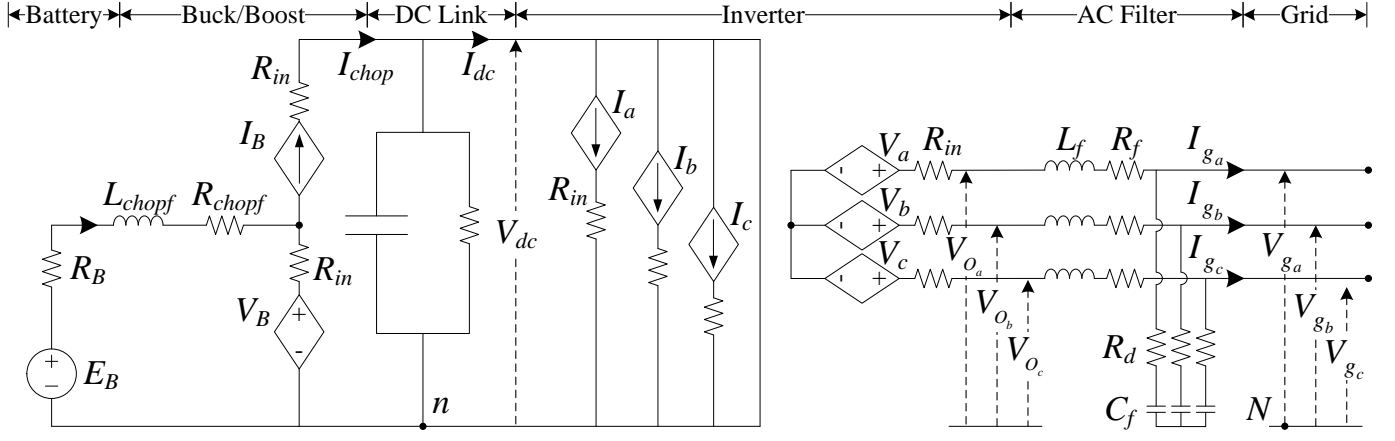


Fig. 8. Schematic of a battery energy storage system with switches being replaced by dependent sources.

TABLE I  
ESS DESIGN PARAMETERS

ESS Parameters				
$L_f$	$R_f$	$C_f$	$R_d$	$V_{rateddc}$
0.166 mH	4.2 mΩ	626.8 μF	84.7 mΩ	750 v
$C_{dclink}$	$R_B$	$L_{chopf}$	$f_s$	$V_{RMSL-L}$
20 mF	0.2 Ω	3.3 mH	3 kHz	460 v

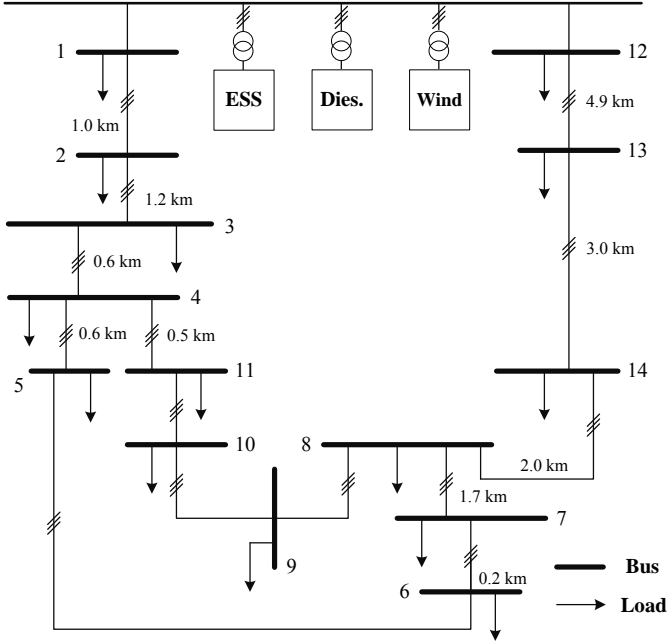


Fig. 9. Modified version of CIGRE benchmark microgrid.

#### A. Case A: Grid-forming BESS in Balanced Operation

In this case, the diesel and wind generators are not connected. The system load is 950 kW of active power and 100 kVar of reactive power, balanced among the three phases; at  $t = 0.5s$ , the load is increased by 100 kVar, and at  $t = 11.5s$ , the reactive power load is again increased by 100 kVar; note that the active power load is near the BESS rated power.

Figure 10 illustrates the active power, reactive power, and

instantaneous voltage of phase a at the PCC for average, ideal dc link, and detailed model. Note in Fig. 10(a), before  $t = 11.5s$ , the battery performance is satisfactory for all the three modeling techniques. Due to switching in the system, there are some fluctuations in the active and reactive power in the ideal dc link and detailed models of the BESS. The Total Harmonic Distortion (THD) of the instantaneous voltage is 0.25% for average model, 3.92% for ideal dc link model, and 3.63% for the detailed model.

After  $t = 11.5s$ , the system remains stable for the average and ideal dc link models, whereas it shows unsustained oscillations for the detailed model. This is due to the fact that as the apparent power demand increases, the charging/discharging current of the dc link capacitor also increases, and beyond a certain value, the dc link capacitor voltage ripple becomes significant, leading to system instability, as illustrated in Fig. 11. Note that the chosen dc link capacitor is relatively large for a 1 MW BESS, and the active power is within the range for which the system is designed. Also, observe that the voltage magnitudes at the PCC are close to their nominal values in the average and ideal dc link models, as compared to the detailed model of the BESS.

Figure 12 shows the BESS active power, reactive power, phase a RMS voltage at PCC, and the dc link voltage for the Average and Switching DSMs. Observe that the performance of the Average DSM is exactly the same as the performance of the average model shown in Fig. 10, and the performance of the Switching DSM is exactly the same as the performance of the detailed model. These models are used in Section V to isolate and evaluate the impact of high frequency switching on the stability of the microgrid.

#### B. Case B: Grid-forming BESS in Unbalanced Operation

In this case, the diesel and wind generators are not connected. The system load is 950 kW of active power and 100 kVar of reactive power, with the load on phase c being twice the load on phase a and b.; at  $t = 0.5s$ , the load is increased by 100 kVar.

Figure 13 presents the active power, reactive power, and RMS phase voltages at the PCC. As seen from Fig. 13, the

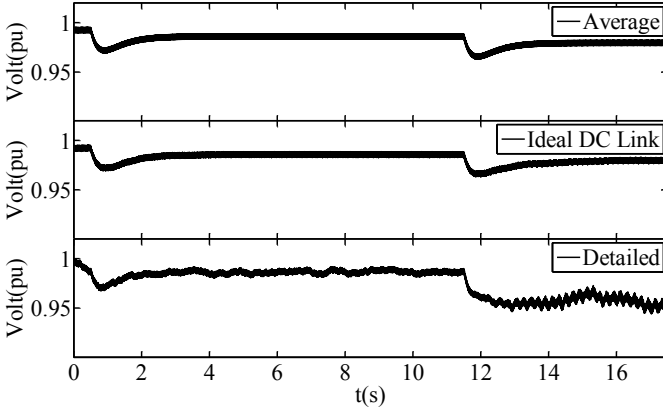
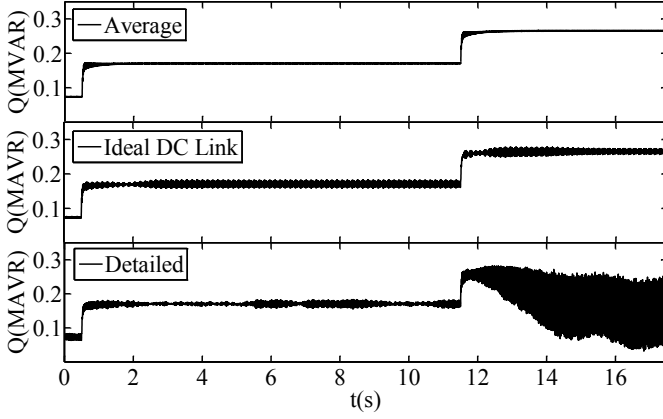
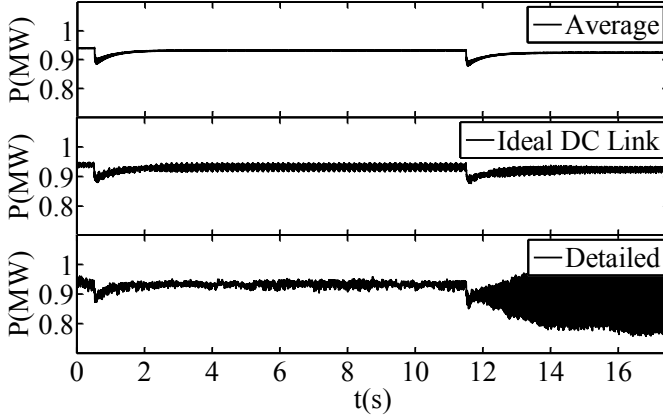


Fig. 10. Case A: (a) Active power, (b) reactive power, and (c) phase *a* RMS voltage at the PCC.

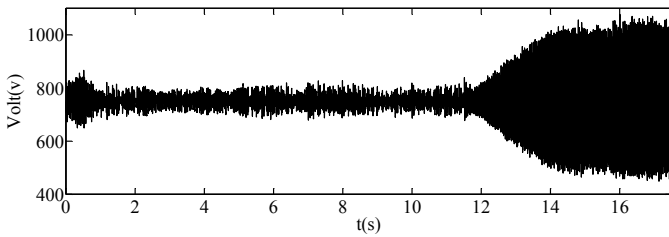


Fig. 11. DC link voltage for the detailed model for Case A.

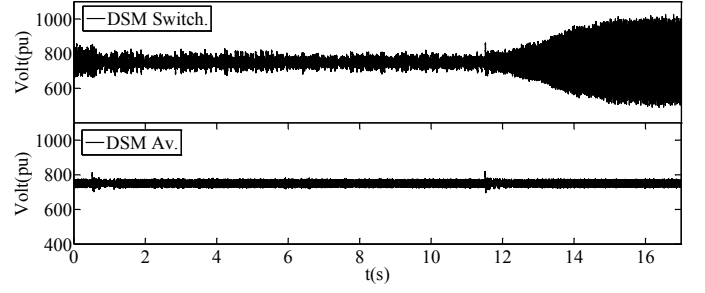
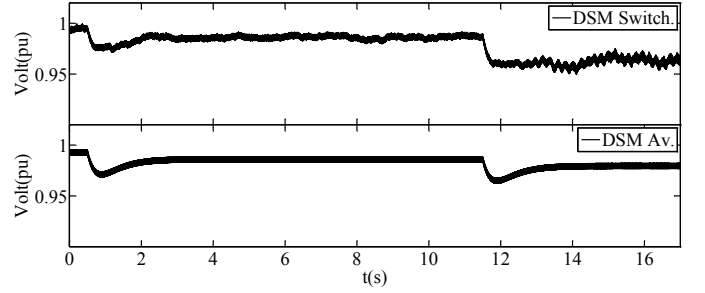
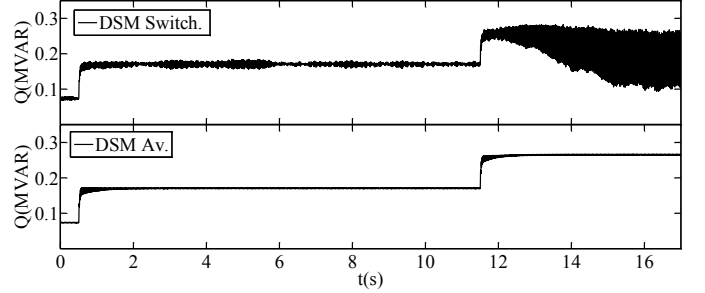
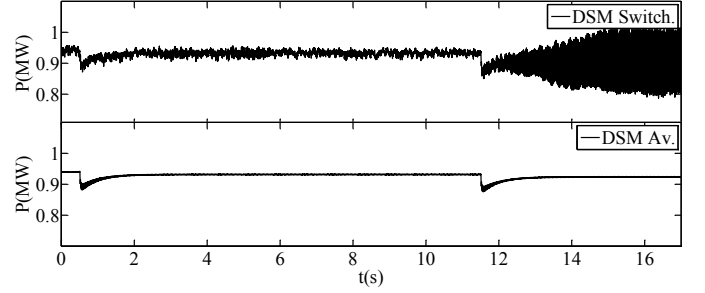
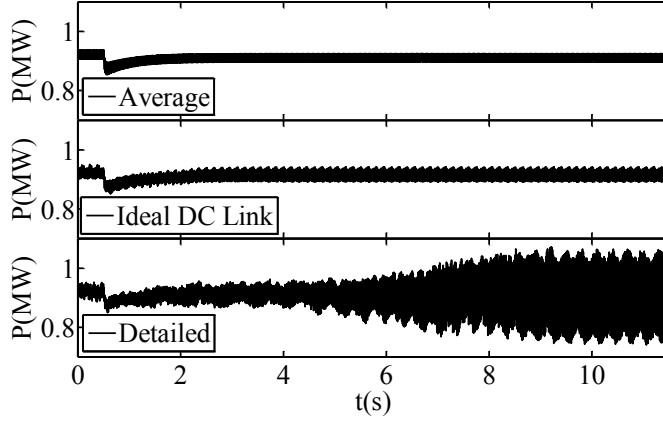


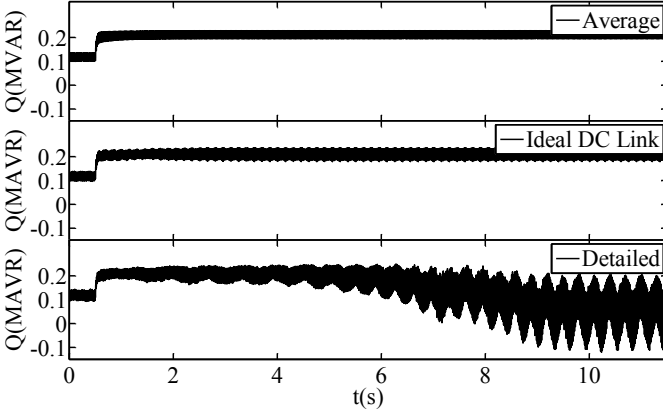
Fig. 12. DSM Case A: (a) Active power; (b) reactive power; (c) phase *a* RMS voltage at PCC, and (d) dc link voltage.

system remains stable after the disturbance for the average and ideal dc link BESS models; however, the system shows unsustained oscillations for the detailed model, since similar to Case A, the dc link capacitor voltage ripples cause the system instability, showing a similar behaviour as in Fig. 11. Comparing Case A and Case B for the same loading condition, it is noted that the same disturbance makes the unbalanced system unstable, whereas the balanced system remains stable.

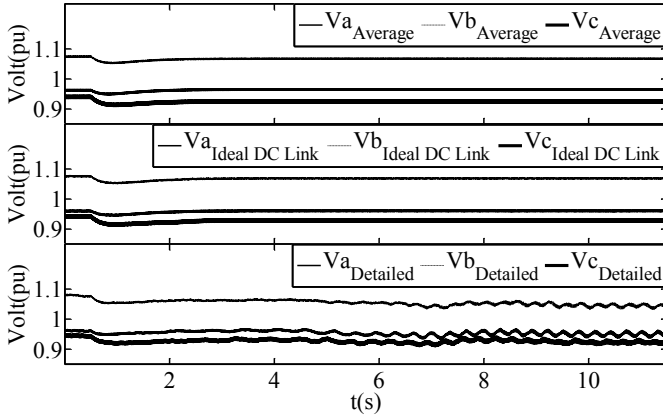
The performance of the Average DSM has found to be exactly the same as the performance of the average model, and



(a)



(b)



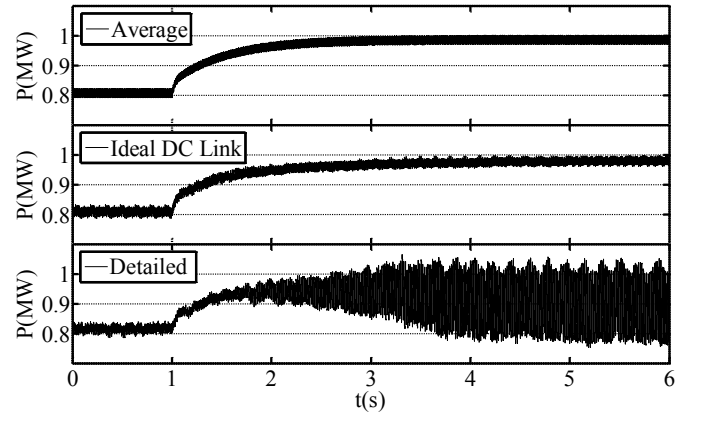
(c)

Fig. 13. Case B: (a) Active power, (b) reactive power, and (c) RMS phase voltages at the PCC.

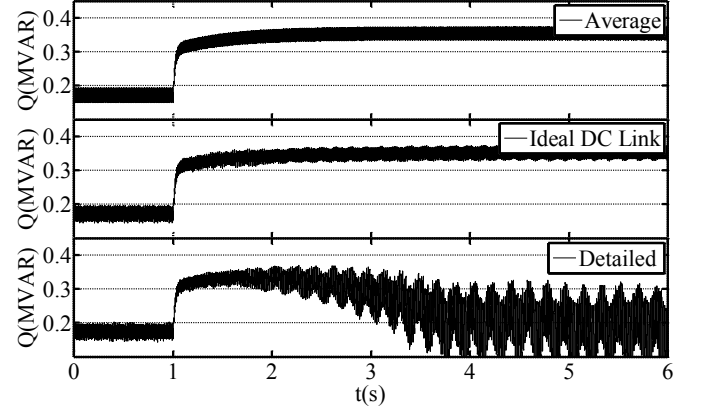
the same for the performance of the Switching DSM compared to the detailed model. Hence, these plots are not shown here.

### C. Case C: Grid-forming BESS with Wind Generator Outage

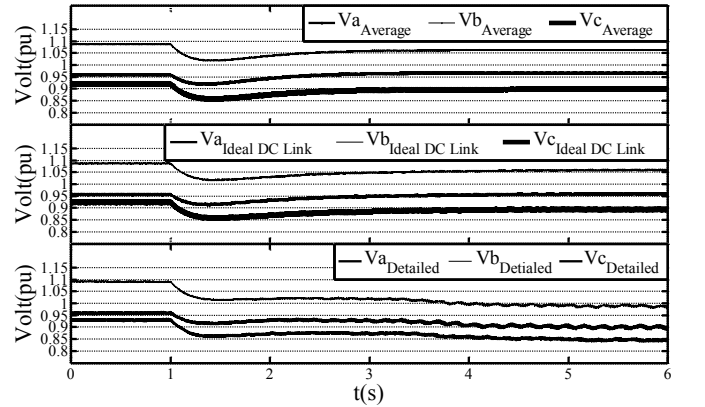
In this case, the diesel generator is not connected, and the wind turbine is generating a constant 200 kW of active power and 200 kVar of reactive power; at  $t = 1$ s, the wind generator is disconnected. The system active power load is 1 MW and reactive power load is 350 kVar, with the load on phase  $c$  being twice the load on phase  $a$  and  $b$ .



(a)



(b)



(c)

Fig. 14. Case C: (a) Active power, (b) reactive power, and (c) phase RMS voltages at the PCC.

Figure 14 illustrates the active power, reactive power, and RMS phase voltages at the PCC. Note that the system remains stable for the average and ideal dc link models, but shows unsustained oscillations for the detailed model. Similar to Case B, the dc link capacitor voltage ripple becomes greater than what the system is designed for, after the wind generator is disconnected.

The performance of the Average DSM has found to be exactly the same as the performance of the average model, and the same for the performance of the Switching DSM compared



to the detailed model. Hence, these plots are not shown here.

#### D. Case D: Grid-supporting BESS With Wind Generator Outage

In this case, the diesel generator is connected and is the master voltage and frequency controller, with the governor and excitation controls, and the BESS is providing 1 MW of active power and half of the system reactive power demand. The wind turbine is generating 500 kW of active power and 500 kVar of reactive power, and the load active power is 2.1 MW and the reactive power is 1 MVar, balanced among the three phases. At  $t = 1$ s, the wind generator is tripped, and at  $t = 7$ s, the load reactive power is increased by 500 kVar.

Figure 15 shows the BESS active power, reactive power, and RMS voltages at the PCC. The diesel generator active and reactive power, and the system frequency are illustrated in Fig. 17. As seen from these figures, the system is able to retain its stability for the average and ideal dc link BESS models after the wind generator is disconnected, i.e between  $t = 1$ s to  $t = 7$ s; however, the system loses its stability for the detailed BESS model. In fact, since the battery has to increase its reactive power generation after the disturbance, it passes a point where the dc link voltage cannot be maintained any longer; as a result, the battery active power generation also shows large unsustained oscillations. Consequently, the diesel generator is not able to meet the demand level and the system frequency, and voltage collapses. The battery dc link voltage for the detailed BESS model is shown in Fig. 16.

After the load reactive power is increased at  $t = 7$ s, the system continues to remain stable for the average model of the BESS, but the system loses stability for the ideal dc link model. This is an important observation, since the only difference between these two models is the presence of switches.

The response of the Average DSM has found to be exactly the same as the performance of the average model. The BESS and diesel engine response of the Switching DSM is shown in Fig. 18 and Fig. 19. Observe that similarly to the detailed model, the Switching DSM becomes unstable after the disturbance at  $t = 1$  s. However, its response is not exactly the same as the detailed model, due to the different modeling approaches; nevertheless, in both cases the system is unstable, and thus they both lead to the same conclusions.

## V. ANALYSIS

In the previous section, it was shown that when the system was pushed to its loading limits, different BESS models demonstrated significantly different performances. These differences can be due to three main factors: the dc-link voltage dynamic, the high frequency switching, and the internal resistance of the switches. To effectively isolate the impact of each factor, first, an eigenvalue study is performed based on a signal-processing technique using the dc-link voltage signal. Second, the proposed DSM is used to eliminate the higher frequencies and investigate the performance of the system. Additionally, the proposed models are compared in terms of the simulation computation times.

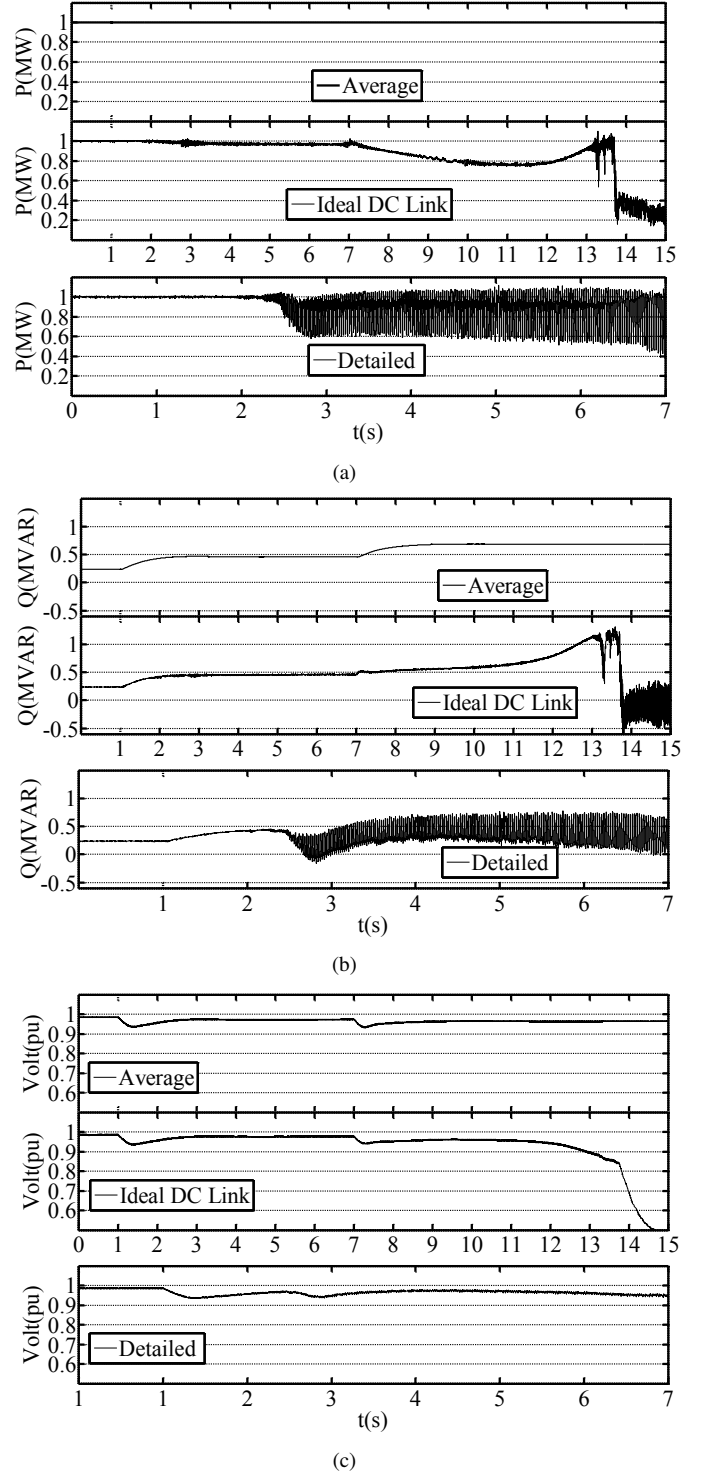


Fig. 15. Case D: BESS (a) Active power, (b) reactive power, and (c) RMS phase voltages at the PCC.

#### A. Small-Signal Analysis

Typically, in conventional power systems, eigenvalue analysis is carried out by linearization of the power system model around an equilibrium point [21]. Such an approach requires considerable simplifications limited to balanced systems, or the development of detailed linearized models of the system [22], which may not be feasible in practical systems. In this

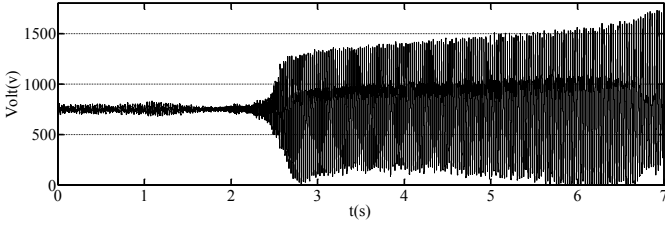


Fig. 16. DC link voltage for the detailed model - Case D.

paper, a modal estimation approach is utilized to identify the dominant eigenvalue of the system [23], [24]. In particular, the Steiglitz-McBride technique is utilized to identify the dominant eigenvalue of the system [25], [26].

To investigate the impact of dc-link voltage dynamics, the dc-link voltage signal of the detailed model in Case A is used to identify the critical eigenvalues before and after the second disturbance, using the MATLAB built-in Steiglitz-McBride function [27]. The critical eigenvalues of the system are shown in Fig. 20, where it can be observed that the dominant eigenvalues are pushed to the right half plane after the second disturbance, resulting in the undamped oscillations in Fig. 11.

### B. Dynamic Analysis

Without loss of generality, the performance of Switching DSM and Average DSM are compared for Case A only in Fig. 12. Note that the behaviour of the Switching DSM is exactly the same as the performance of the detailed model shown in Fig. 10; thus, by comparing the performance of the Switching and Average DSMs, it is possible to isolate the impact of high-frequency switching due to the switches, since the physical components of both DSMs are all the same, since only the values of the coefficients of the dependent sources in (13), (14), (19), and (21) are different, reflecting the different switching content in the two models. As seen in Fig. 12, the performance of the Average DSM is the same as the performance of the average model, showing that including the dc link dynamics is not necessary in average modeling approaches; furthermore, it confirms that it is not possible to capture the behaviour of the detailed model by neglecting the switches and/or the impact of high-frequency switching. In addition, it can be concluded that including the dc link voltage dynamics is necessary but not sufficient to capture the accurate dynamic performance of the system.

With the Switching DSM, it is also possible to isolate and investigate the impact of  $R_{in}$  on the system's performance. Thus, it was found that eliminating  $R_{in}$  has no considerable impact on the performance of Switching DSM. Hence, it can be concluded that the internal resistance of the switches does not significantly contribute to the differences in the performance of the different models.

### C. Computation Times

The simulation times in Case A are compared for the proposed BESS models in Table II. The simulations were

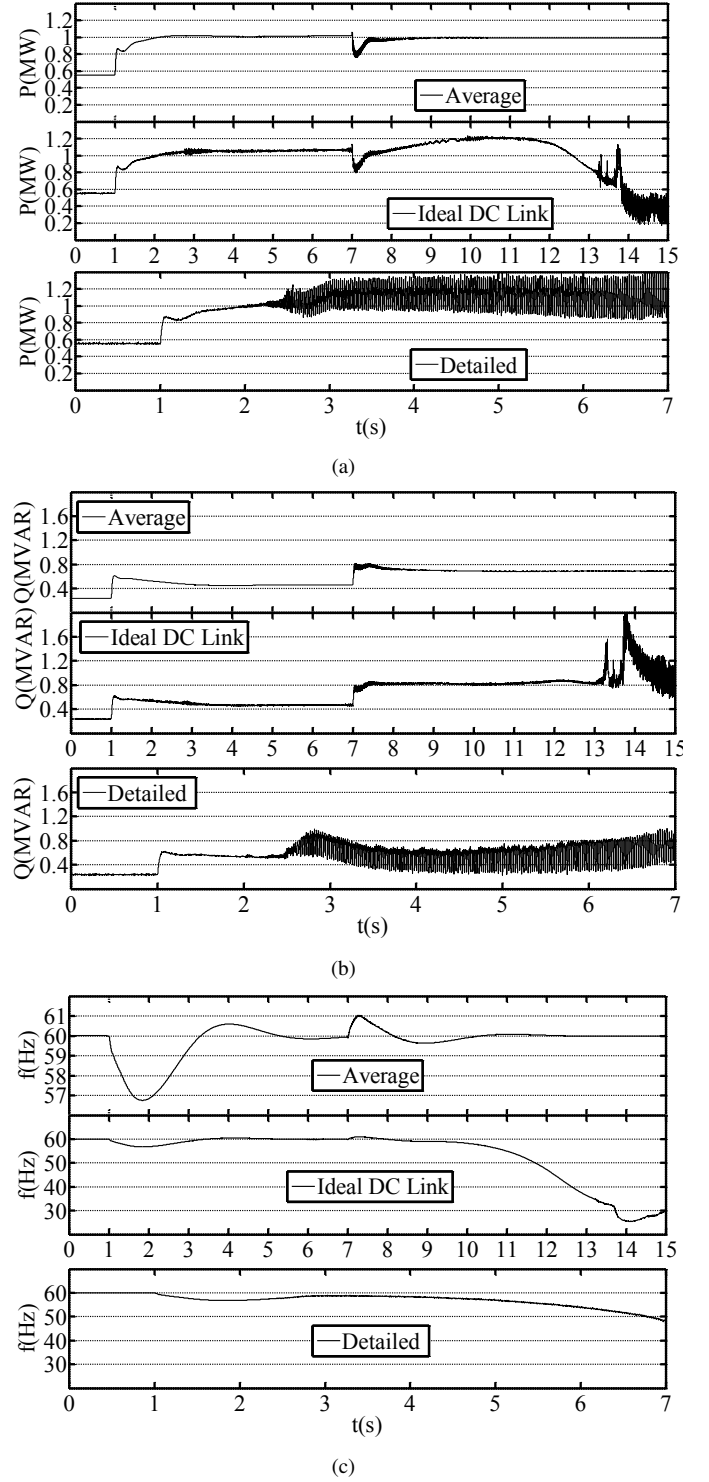


Fig. 17. Case D: Diesel generator (a) active power; (b) reactive power; and (c) system frequency.

performed in PSCAD/EMTDC 4.6.1.0 on a PC with an Intel(R) Xeon(R) CPU consisting of four 1.86 GHz processors, and 64 GB RAM. The computation times were obtained by averaging waiting times for multiple 1 s simulation times, under similar server conditions, for the different models in the same scenario. Note that the Switching DSM is faster than the detailed model, while capturing its behaviour. Considering that

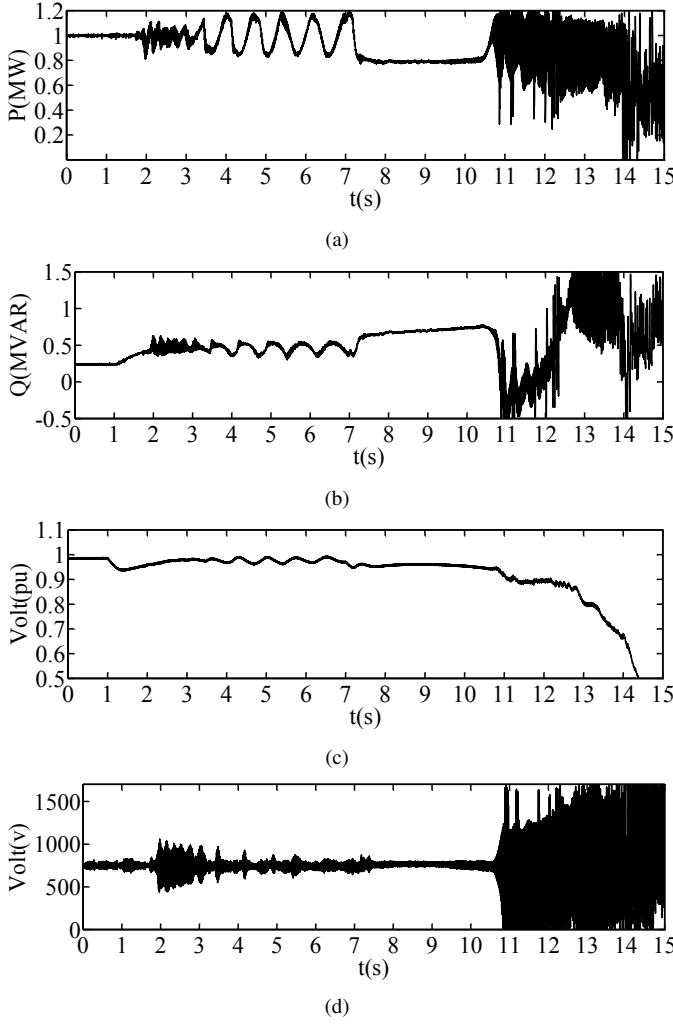


Fig. 18. Switching DSM Case D: BESS (a) active power, (b) reactive power, (c) RMS phase voltages at the PCC, and (d) dc-link voltage.

TABLE II

AVERAGE COMPUTATION TIMES OF 1 s OF SIMULATION TIME IN CASE A

Detailed	Ideal dc	Average	Switch. DSM	Av. DSM
50.6 s	43.4 s	24.8 s	39.4 s	27.0 s

the difference in computation times increases exponentially as the number of inverters in the system increases, those can become more considerable for larger systems. Finally, note that the Average DSM is slightly slower than the average model, yielding essentially the same performance.

## VI. CONCLUSIONS

In this paper, first, three different BESS models were presented and discussed: an average model that replaced the switches with ac voltage sources, an ideal dc link model in which the battery and buck/boost converter were replaced by an ideal dc voltage source, and a detailed model that included all necessary modeling and control details. In addition, to isolate and investigate the impact of high-frequency harmonics caused by switchings, a new model was proposed in which the switches were replaced by dependent voltage and current sources, to capture the average and the fast switching

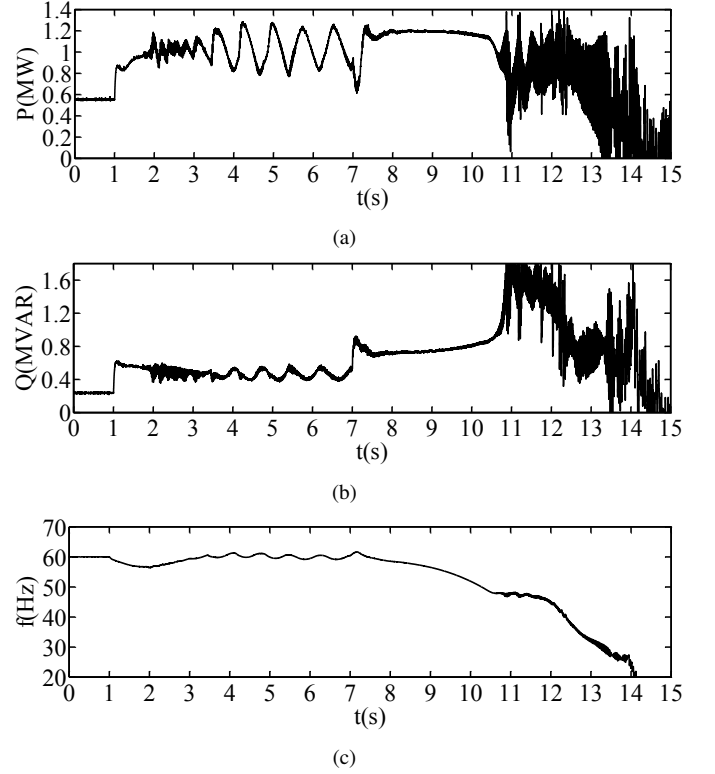


Fig. 19. Switching DSM Case D: diesel generator (a) active power; (b) reactive power; and (c) system frequency.

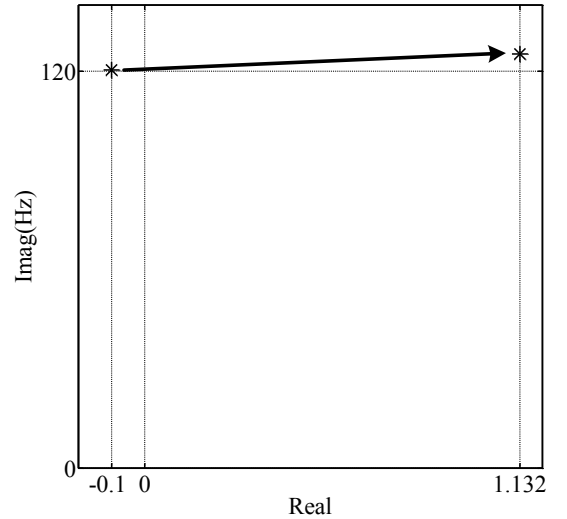


Fig. 20. Dominant eigenvalue before and after instability in Case A.

behaviour of other models at adequate computational performance.

The following can be concluded from the presented studies:

- During normal operating conditions, little differences were observed between different models performances; the THD were higher for the fast-switching and ideal dc link models compared to the average models, due to the switching in the system
- When the system loading was pushed to its limits, the fast-switching models lost their stability, while the ideal

dc link model and the average models remained stable. Also, it was demonstrated that the ideal dc link model lost its stability for certain loading levels for which the average models remained stable.

- Through eigenvalue studies, it was observed that dc link dynamics contribute to the instability problem observed in the fast-switching modelings, due to the increase in charging/discharging current of the dc link capacitor.
- By comparing the performance of the DSMs, it can be concluded that including the dc link voltage dynamics is a necessary but not sufficient condition to capture the accurate performance of the system. It was revealed that high-frequency dynamics also contribute the instability phenomena observed in the test scenarios.
- It was shown that the internal resistance of the switches is not a major factor in the dynamic performance of the system.
- Comparing the computation time of the models, it was noted that during normal operating conditions, it may not be necessary to include the dc link dynamics in averaging models. Thus, it can be concluded that when the BESS is in normal operating conditions, the average model is the best option, since it significantly saves simulation time speed, exhibiting adequate performance. However, if the BESS operates in grid-forming/grid-supporting modes, and the system is heavily loaded or unbalanced, using average or ideal dc link models, or any other model that neglects the dc link voltage dynamics and/or the high frequency switching, do not properly capture the BESS behaviour during or after a disturbance.

## REFERENCES

- [1] R. H. Lasseter *et al.*, "CERTS microgrid laboratory test bed," *IEEE Trans. Power Del.*, vol. 26, pp. 325–332, Jan. 2011.
- [2] *IEEE Guide for Design, Operation, and Integration of Distributed Resource Island Systems with Electric Power Systems*, IEEE Std. 1547.4, 2011.
- [3] J. M. Guerrero, F. Blaabjerg, T. Zhelev, K. Hemmes, E. Monmasson, S. Jemei, M. P. Comech, R. Granadino, and J. I. Frau, "Distributed generation: toward a new energy paradigm," *IEEE Ind. Electron. Mag.*, pp. 52–64, March 2010.
- [4] G. Delille, B. Francois, G. Malarange, and J.-L. Fraise, "Energy storage systems in distribution grids: New assets to upgrade distribution network abilities," in *Proc. 20<sup>th</sup> International Conf. and Exhibition on Electricity Distribution (CIRED) - Part I*, Prague, Czech Republic, June 2009.
- [5] G. Delille, B. Francois, and G. Malarange, "Dynamic frequency control support by energy storage to reduce the impact of wind and solar generation on isolated power system's inertia," *IEEE Trans. Sustain. Energy*, vol. 3, no. 4, pp. 931–939, Nov. 2012.
- [6] A. Ortega and F. Milano, "Generalized model of VSC-based energy storage systems for transient stability analysis," *IEEE Trans. Power Syst.*, vol. 21, no. 5, pp. 3369–3380, Sep. 2016.
- [7] F. A. Inthamoussou, J. Peguerles-Queralt, and F. D. Bianchi, "Control of a supercapacitor energy storage system for microgrid applications," *IEEE Trans. Energy Convers.*, vol. 28, no. 3, pp. 690–697, Sep. 2013.
- [8] J. Wu, J. Wen, H. Sun, and S. Cheng, "Feasibility study of segmenting large power system interconnections with AC link using energy storage technology," *IEEE Trans. Power Syst.*, vol. 27, no. 3, pp. 1245–1252, Aug. 2012.
- [9] J. Fang, W. Yao, Z. Chen, J. Wen, and S. Cheng, "Design of anti-windup compensator for energy storage-based damping controller to enhance power system stability," *IEEE Trans. Power Syst.*, vol. 29, no. 3, pp. 1175–1185, May 2014.
- [10] Z. Jankovic, B. Novakovic, V. Bhavaraju, and A. Nasiri, "Average modeling of a three-phase inverter for integration in a microgrid," in *Proc. IEEE Energy Conversion Congress and Exposition*, Milwaukee, WI, Nov. 2014.
- [11] J. W. Choi and S. K. Sul, "Inverter output voltage synthesis using novel dead time compensation," *IEEE Trans. Power Electron.*, vol. 11, no. 2, pp. 221–227, Mar. 1996.
- [12] Y. Wang, G. Delille, X. Guillaud, F. Colas, and B. Francois, "Real-time simulation: The missing link in the design process of advanced grid equipment," in *Proc. IEEE Power and Energy Soc. Gen. Meeting*, Minneapolis, MN, July 2010.
- [13] O. Tremblay, L.-A. Dessaint, and A. Dekkiche, "A generic battery model for the dynamic simulation of hybrid electric vehicles," in *Proc. IEEE Vehicle Power and Propulsion Conference*, Arlington, TX, Sep. 2007.
- [14] S. Koenig, P. Muller, and T. Leibfried, "Design and comparison of three different possibilities to connect a vanadium-redox-flow-battery to a wind power plant," in *Proc. 13<sup>th</sup> CHLIE*, Valencia, Spain, July 2013.
- [15] S. M. Ashabani and Y. A. R. I. Mohamed, "New family of microgrid control and management strategies in smart distribution grids - analysis, comparison and testing," *IEEE Trans. Power Syst.*, vol. 29, no. 5, pp. 2257–2269, Sep. 2014.
- [16] M. Liserre, F. Blaabjerg, and S. Hansen, "Design and control of an Lcl-filter-based three phase active rectifier," *IEEE Trans. Ind. Appl.*, vol. 41, no. 5, pp. 1281–1291, Sep. 2005.
- [17] M. Restrepo, J. Morris, M. Kazerani, and C. Canizares, "Modeling and testing of a bidirectional smart charger for distribution system ev integration," *IEEE Trans. Smart Grid*, vol. PP, no. 99, pp. 1–11, Mar. 2016.
- [18] K. Strunz, "Developing benchmark models for studying the integration of distributed energy resources," in *Proc. IEEE Power Eng. Soc. Gen. Meeting*, Montreal, QC, July 2006.
- [19] M. Arriaga and C. A. Cañizares, "Overview and analysis of data for microgrid at kasabonika lake first nation (KLFN)," Hatch Project Confidential Report, University of Waterloo, Tech. Rep., Sep. 2015.
- [20] G. Delille, L. Capely, D. Souque, and C. Ferrouillat, "Experimental validation of a novel approach to stabilize power system frequency by taking advantage of load voltage sensitivity," in *Proc. IEEE PowerTech*, Eindhoven, June 2015.
- [21] P. Kundur, *Power System Stability and Control*. New York, US: McGraw-hill Professional, 1994.
- [22] R. H. Salim and R. A. Ramos, "A model-based approach for small-signal stability assessment of unbalanced power systems," *IEEE Trans. Power Syst.*, vol. 27, no. 4, pp. 1184–1190, Nov. 2012.
- [23] R. H. Salim, R. A. Ramos, and N. G. Bretas, "Analysis of the small signal dynamic performance of synchronous generators under unbalanced operating conditions," in *Proc. IEEE Power Eng. Soc. Gen. Meeting*, Minneapolis, MN, July 2010.
- [24] E. Nasr-Azadani, C. A. Canizares, D. E. Olivares, and K. Bhattacharya, "Stability analysis of unbalanced distribution systems with synchronous machine and DFIG based distributed generators," *IEEE Trans. Smart Grid*, vol. 5, no. 5, pp. 2326–2338, Sep. 2014.
- [25] K. Steiglitz and L. E. McBride, "A technique for the identification of linear systems," *IEEE Trans. Automatic Control*, vol. 10, no. 4, pp. 461–464, Oct. 1965.
- [26] L. Ljung, *System Identification: Theory for the User*. Upper Saddle River, NJ: Prentice Hall, 1998.
- [27] Matlab mathworks inc. [Online]. Available: <https://www.mathworks.com/products/matlab.html>

**Mostafa Farrokhabadi** (S'10) received his B.Sc. in Electrical Engineering from Amirkabir University of Technology, Tehran, Iran, in 2010, his M.Sc. in Electric Power Engineering from KTH Royal Institute of Technology, Stockholm, Sweden, in 2012, and his Ph.D. in Electrical and Computer engineering from the University of Waterloo, ON, Canada, in 2017. He is currently a postdoctoral fellow at the Electrical and Computer Engineering Department of the University of Waterloo. His research interests includes modeling, control, and optimization in microgrids, mathematical modeling, and state estimation.

**Sebastian König** (M'17) received the Dipl.-Ing. and Dr.-Ing. degrees from the Karlsruhe Institute of Technology, Karlsruhe, Germany, in 2011 and 2017, respectively. His current research interest is electric energy storage and its grid integration. In his PhD thesis, he presents a model-based design and optimization approach for the Vanadium Redox Flow Battery.

**Claudio Cañizares** (S'85-M'91-SM'00-F'07) is a Full Professor and the Hydro One Endowed Chair at the Electrical and Computer Engineering (E&CE) Department of the University of Waterloo, where he has held various academic and administrative positions since 1993. He received the Electrical Engineer degree from the Escuela Politécnica Nacional (EPN) in Quito-Ecuador in 1984, where he held different teaching and administrative positions between 1983 and 1993, and his MSc (1988) and PhD (1991) degrees in Electrical Engineering are from the University of Wisconsin-Madison. His research activities focus on the study of stability, modeling, simulation, control, optimization, and computational issues in large and small grids and energy systems in the context of competitive energy markets and smart grids. In these areas, he has led or been an integral part of many grants and contracts from government agencies and companies, and has collaborated with industry and university researchers in Canada and abroad, supervising/co-supervising many research fellows and graduate students. He has authored/co-authored a large number of journal and conference papers, as well as various technical reports, book chapters, disclosures and patents, and has been invited to make multiple keynote speeches, seminars, and presentations at many institutions and conferences world-wide. He is an IEEE Fellow, as well as a Fellow of the Royal Society of Canada, where he is currently the Director of the Applied Science and Engineering Division of the Academy of Science, and a Fellow of the Canadian Academy of Engineering. He is also the recipient of the 2017 IEEE Power & Energy Society (PES) Outstanding Power Engineering Educator Award, the 2016 IEEE Canada Electric Power Medal, and of various IEEE PES Technical Council and Committee awards and recognitions, holding leadership positions in several IEEE-PES Technical Committees, Working Groups and Task Forces.

**Kankar Bhattacharya** (M95-SM01-F17) received the Ph.D. degree in electrical engineering from the Indian Institute of Technology, New Delhi, India, in 1993. He was in the faculty of Indira Gandhi Institute of Development Research, Mumbai, India, from 1993 to 1998, and the Department of Electric Power Engineering, Chalmers University of Technology, Gothenburg, Sweden, from 1998 to 2002. In 2003, he joined the Electrical and Computer Engineering Department, University of Waterloo, Waterloo, ON, Canada, where he is currently a Full Professor. His current research interests include power system economics and operational aspects.

**Thomas Leibfried** (M'96) received the Dipl.-Ing. and Dr.-Ing. degrees from the University of Stuttgart, Stuttgart, Germany, in 1990 and 1996, respectively. From 1996 to 2002, he was with Siemens AG, working in the power transformer business in various technical and management positions. In 2002, he joined the Karlsruhe Institute of Technology, KIT as Head of the Institute of Electric Energy Systems and High-Voltage Technology. He is the author of various technical papers. Prof. Leibfried is a member of VDE and CIGRE.